Diagrammatic method for investigating universal behavior of impurity systems

Kurt Fischer
Max-Planck-Institut für Physik komplexer Systeme, Bayreuther Strasse 40, 01187 Dresden, Germany
(Received 18 November 1996; revised manuscript received 31 January 1997)

The universal behavior of magnetic impurities in a metal is proved with the help of skeleton diagrams. The energy scales are derived from the structure of the skeleton diagrams. A minimal set of skeleton diagrams is sorted out that scales exactly. For example, the noncrossing approximation (NCA) for the Anderson impurity model can describe the crossover phenomenon. The universal Wilson-number is calculated within the NCA. The method allows for an assessment of various approximations for impurity Hamiltonians.
[S0163-1829(97)06520-X]

I. INTRODUCTION

Magnetic impurities in metals show a universal behavior at low energies.[1] The Hamiltonian of such systems consists of at least one conduction band of width D to which the impurity couples.[2] At temperatures $k_BT \ll D$, the scaled observable is independent of details of the host system such as its band structure.

A long standing question in the physics of such systems is: How can the observed universal behavior directly be established from the original model Hamiltonian such as the Anderson-impurity model,[2] together with a reasonable accurate description of observables? Hitherto the original Hamiltonian has been replaced by another one which is more accessible.

(a) Within the Bethe ansatz the impurity part of the system's thermodynamics can be derived. However, the original model has to be replaced by one with linear dispersion. The spectrum of eigenvalues is cut off at D', which is in general *not* identical with the bandwidth D of the metallic host in the original model.[3,4] A relation between D and D' has so far been established only for the Anderson impurity model.[5]

(b) Within the numerical renormalization group,[6] the impurity is coupled to a half-infinite chain with hopping matrix elements vanishing as $\Lambda^{-n}, n=1,2,\ldots,\Lambda>1$. In the limit of $\Lambda=1$ one would recover the original model. However, the numerical results have to be extrapolated to that limit because the length of the chain to be diagonalized numerically would eventually become too large.[2,6]

Hence both methods do not prove that the observables of the original model behave universally. On the other hand, there are the diagrammatic approaches to the impurity problem.[7] They allow us to construct approximations for all observables of the original model. The Dyson equation

$$R^{-1}(z)=R_0^{-1}(z)-\Sigma(z)$$

is invariant under a certain rescaling of the propagators R and R_0, self-energies Σ, and coupling constants. With the help of the diagrammatic renormalization group, perturbative results for the propagators, self-energies, and vertex parts are then fitted to the Dyson equation. In that way, scaling laws for the propagators result, from which the universal behavior in the perturbative high-energy regime of the model[8] follows. This method amounts to summing a certain subclass of diagrams, with *naked* propagators. However, the procedure breaks down when perturbation theory fails.

For the nonperturbative region *dressed* propagators are necessary. This requires the use of skeleton diagrams, otherwise the definition of a self-energy itself would become ambiguous. However, the scaling of the dressed propagators is unknown, precisely because beforehand the Dyson equation would have to be solved.

In this paper, this difficulty is overcome by utilizing the variational principle of Luttinger and Ward,[9] Kuramoto,[10] and Baym,[11] by which any observable can be expressed in terms of skeleton diagrams. This is exemplified at the Anderson-impurity Hamiltonian.

It turns out that the skeleton diagrams of the second order are already sufficient to calculate the exact energy scales. This proves a universal behavior for this model. The second-order skeleton diagrams are therefore the minimal class of diagrams which have to be summed, in order to describe the crossover.

II. HAMILTONIAN AND DIAGRAM TECHNIQUE

As the standard model describing magnetic impurities in metals, the Anderson-impurity Hamiltonian[2] is considered, with a half-filled conduction band of constant density of states ρ and infinite Coulomb repulsion at the impurity site:

$$\begin{aligned} H&=H_c+H_f+H_1,\\ H_c&=\sum_{|\epsilon_p|\le D,m}\epsilon_p c_{pm}^{+}c_{pm},\\ H_f&=\epsilon_f\sum_m f_m^{+}f_m,\\ H_1&=\frac{V}{\sqrt{N}}\sum_{p,m}(c_{pm}^{+}b^{+}f_m+\text{H.c.}). \end{aligned} \tag{1}$$

c_{pm}^{+} creates a conduction electron with internal quantum number $m=1\ldots N$, momentum p, and energy ϵ_p which is cut off at $\pm D$. $|m\rangle=f_m^{+}|\text{vac}\rangle$ denotes a magnetic configuration of the impurity and $|0\rangle=b^{+}|\text{vac}\rangle$ the nonmagnetic one, their energy-difference being ϵ_f. f_m^{+} is a fermionic operator and b^{+} the Coleman boson.[12] $F_m^{+}=f_m^{+}b$ creates an electron

at the impurity site. Double occupancy at the impurity site is suppressed by imposing the constraint $n_b+n_f=1$. The impurity hybridization with the conduction band is proportional to V. The Boltzmann constant is set to unity, so that temperature is measured in units of energy.

In order to simplify the subsequent derivations, the conduction band of model (1) is assumed to have a constant density of states ρ with a sharp cutoff at energies $\pm D$, as the other approaches to scaling do.[2,3,8] Universal behavior should not depend on this assumption.[3] In Sec. VII it will be shown that the energy scales of the system indeed do not change as long as the density of states is finite at the Fermi energy, and is sufficiently structureless to have only one energy scale D.

The principal object of concern is the resolvent $R_f(z)=\langle Q(z)\rangle_c$, where Q is defined as

$$Q(z)=1/(z-L_c-H_f-H_1).$$

Here the superoperator L_c acts on an operator X of the Hilbert space as $L_cX=[H_c,X]$, and $\langle\ \rangle_c$ indicates the thermodynamic average with respect to H_c. The propagators for the occupied and unoccupied ionic configurations are

$$R_m(z):=\langle m|R_f(z)|m\rangle,$$

$$R_0(z):=\langle 0|R_f(z)|0\rangle.$$

With the help of the identity[13]

$$e^{-\beta H}=e^{-\beta(L_c+H_f+H_1)}e^{-\beta H_c}, \tag{2}$$

the impurity part Z_f of the partition function can then be represented as a line integral, the path of integration encircling all poles of the integrand:

$$Z_f:=\frac{\mathrm{Tr}_f\mathrm{Tr}_c e^{-\beta H}}{\mathrm{Tr}_c e^{-\beta H_c}}=\mathrm{Tr}_f\oint\frac{dz}{2\pi i}e^{-\beta z}R_f(z). \tag{3}$$

The well-known diagrammatic technique[14] follows if Q is expanded in a geometric series in V; then L_c acting on the conduction-electron operators in H_1 is evaluated to give the energy denominators

$$L_c(c^+_{pm}c_{qn}\ldots)=(\epsilon_p-\epsilon_q+\cdots)(c^+_{pm}c_{qn}\ldots),$$

and finally Wick's theorem applied to evaluate the thermodynamic average with respect to H_c. This can be casted in a diagrammatic language. The naked propagators and vertices are shown in Fig. 1. Because the impurity site can alternatively be empty or singly occupied, every diagram has a spine of alternating b and f propagators. Consequently, all diagrams where a conduction-electron propagator would have a self-energy are excluded,[14] because they do not fulfill the constraint $n_b+n_f=1$. Alternative approaches where this constraint is not exactly enforced will be discussed in Sec. VIII.

Within the variational principle,[9,11] a functional Υ of the dressed one-particle propagators is defined. Because the conduction-electron propagators carry no self-energy, the variational principle has been adapted to the present diagrammatic technique[10] such that Υ becomes a functional of the dressed one-particle impurity-propagators only. At the saddle point with respect to variations of the $R_{0,m}$, the functional Υ equals Z_f, and the Dyson equation holds as a self-consistency equation[10]

FIG. 1. Vertices for the Anderson model. A dashed line represents the naked propagator of the occupied f^1 configuration with internal quantum number m. A wavy line represents the naked propagator of the unoccupied f^0 configuration. A solid line represents the propagator of a conduction electron with internal quantum number m. Every diagram has a spine of alternating wavy and dashed impurity propagators. The conduction-electron propagators carry no self-energy (Ref. 14).

$$R_f(z)^{-1}=z-H_f-\Sigma_f(z). \tag{4}$$

For the impurity part of the partition function, the functional is given by

$$\Upsilon=\beta\ \mathrm{Tr}_f\oint\frac{dz}{2\pi i}e^{-\beta z}\left\{\sum_n\left(1-\frac{1}{n}\right)\Sigma_f^{(n)}(z)R_f(z)+\ln\left[z-H_f-\sum_n\Sigma_f^{(n)}(z)\right]\right\}. \tag{5}$$

Here $\Sigma_f^{(n)}$ denotes all nth-order self-energy diagrams of R_f, expressed in terms of skeleton diagrams. Skeleton diagrams are diagrams where all self-energy insertions have been removed. Hence a skeleton diagram becomes a functional of the dressed propagators.

The variational principle can be interpreted in the following fashion: If Υ depends on some parameter λ such as the hybridization then, at the saddle point, it depends on λ only explicitly, and not implicitly via the propagators[10]

$$\frac{d\Upsilon}{d\lambda}=\frac{\partial\Upsilon}{\partial\lambda}+\frac{\delta\Upsilon}{\delta R_{0,m}}\frac{\partial R_{0,m}}{\partial\lambda}=\frac{\partial\Upsilon}{\partial\lambda}.$$

Explicitly, from Eq. (5) it follows at the saddle point that

$$\frac{dZ_f}{d\lambda}=-\frac{d}{d\lambda}\beta\ \mathrm{Tr}_f\oint\frac{dz}{2\pi i}e^{-\beta z}\sum_n\frac{1}{n}\Sigma_f^{(n)}(z)R_f(z)-\frac{d}{d\lambda}\beta\ \mathrm{Tr}_f\oint\frac{dz}{2\pi i}e^{-\beta z}R_f(z)H_f,$$

where the λ dependence of R_f can be discarded.

In order to study the dependence of Z_f on a parameter λ, it therefore suffices to consider all skeleton diagrams of the type $\Sigma^{(n)}_{0,m}R_{0,m}$. A skeleton diagram for $\Sigma_0^{(2)}R_0$, i.e., of second order, is shown in Fig. 2.

Approximations fulfilling the variational principle can be generated by using a subclass, a so-called family of skeleton-diagrams,[15] which contains with each skeleton diagram for

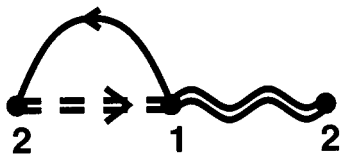

FIG. 2. Skeleton diagram for $\Sigma_0^{(2)}(R_m(z))R_0(z)$. The last vertex can be identified with the first because of the trace over the f configurations in Eq. (5). The double dashed and double wavy lines represent dressed propagators.

$\Sigma_{0,m}^{(n)}R_{0,m}$ all others with cyclic permuted vertices as well. For example, all skeleton diagrams of a given order $\Sigma_{0,m}^{(n)}R_{0,m}$ form such a family.

For instance, if only skeleton diagrams of second order are kept in Eq. (5), this amounts to summing all diagrams with bare propagators and noncrossing conduction-electron lines, and is called the NCA.[10] The self-energies of the NCA, $\Sigma_m^{(2)}(z)=\Sigma_m^{(2)}[R_0(z)]$ and $\Sigma_0^{(2)}(z)=\Sigma_0^{(2)}[R_1(z),\ldots,R_n(z)]$, are then ($f$ denotes the Fermi function)

$$\Sigma_m^{(2)}(z)=\frac{V^2\rho}{N}\int_{-D}^{D}f(\epsilon)R_0(z+\epsilon)d\epsilon, \tag{6}$$

$$\Sigma_0^{(2)}(z)=\frac{V^2\rho}{N}\sum_{m=1}^{N}\int_{-D}^{D}f(\epsilon)R_m(z+\epsilon)d\epsilon.$$

The functional $\Upsilon^{(2)}$ has then the form

$$\Upsilon^{(2)}=\oint\frac{\beta dz}{2\pi i}e^{-\beta z}\left\{\tfrac{1}{2}\Sigma_0^{(2)}(z)R_0(z)+\tfrac{1}{2}\sum_m\Sigma_m^{(2)}(z)R_m(z)\right.$$
$$\left.+\ln[z-\Sigma_0^{(2)}(z)]+\sum_m\ln[z-\epsilon_f-\Sigma_m^{(2)}(z)]\right\}.$$

To construct a variational principle for other observables, the Hamiltonian has to be coupled to external fields suitably chosen.[10] This will be discussed in Sec. V.

III. ENERGY SCALES

A. First scaling equation

Υ as defined in Eq. (5) depends explicitly on ϵ_f only via the term $H_f=\epsilon_f\Sigma_m f_m^+ f_m$. Consequently, one has, for the impurity part $F_f=-T\ln Z_f$ of the free energy,[14]

$$Z_f\epsilon_f\partial_{\epsilon_f}F_f=\mathrm{Tr}_f H_f\oint\frac{dz}{2\pi i}e^{-\beta z}R_f(z). \tag{7}$$

Υ depends explicitly on V via[10] the prefactor V^{2n} of the $2n$th order self-energy $\Sigma_f^{(2n)}$,

$$Z_f\rho V^2\partial_{\rho V^2}F_f=\tfrac{1}{2}\,\mathrm{Tr}_f\oint\frac{dz}{2\pi i}e^{-\beta z}\Sigma_f(z)R_f(z). \tag{8}$$

To determine the T dependence, the internal integration variables z and ϵ as in Eqs. (5) and (6) are replaced by Tz and $T\epsilon$, respectively. The variational principle remains unaffected. Υ depends now explicitly on T via the prefactor T^n of a skeleton diagram of $2n$th order, the term Tz in the logarithm, and the integration boundaries as in Eq. (6) change to $\pm D/T$. Therefore

$$Z_f\left(F_f-T\frac{\partial}{\partial T}F_f\right)=\frac{1}{2}\mathrm{Tr}_f\oint\frac{dz}{2\pi i}e^{-\beta z}\Sigma_f(z)R_f(z)$$
$$+Z_fD\frac{\partial}{\partial D}F_f+\mathrm{Tr}_f H_f\oint\frac{dz}{2\pi i}e^{-\beta z}R_f(z). \tag{9}$$

Inserting Eq. (7) and Eq. (8) into Eq. (9) yields

$$F_f=\left(T\frac{\partial}{\partial T}+\rho V^2\frac{\partial}{\partial\rho V^2}+\epsilon_f\frac{\partial}{\partial\epsilon_f}+D\frac{\partial}{\partial D}\right)F_f. \tag{10}$$

This equation expresses the scaling of F_f with respect to the energy scales D, ϵ_f, and ρV^2:

$$F(T,\rho,V,\epsilon_f,D)=Tf\left(\frac{T}{\rho V^2},\frac{T}{\epsilon_f},\frac{T}{D}\right).$$

This is henceforth called the first scaling equation.

B. Second scaling equation

The central issue of this work is to prove and describe the universal behavior of impurity systems. To show the universal behavior for F_f, the functional Υ is examined for large but finite D; that is, when D becomes larger than all other energy scales of the system, the so-called universal limit.[3]

Υ depends explicitly on the cutoff D only via the integration boundaries $\pm D$ of the integration over the conduction-electron energies, as can be seen in Eq. (6) for the second-order skeleton diagrams.

At first only those second-order self-energies are kept in Υ. With the help of the spectral densities $\rho_{0,m}$ of $R_{0,m}$, one has

$$D\frac{\partial}{\partial D}F_f^{(2)}=\frac{V^2\rho}{NZ_f}\sum_{\substack{m=1\\ \mu=\pm1}}^{N}\int e^{-\beta\omega}d\omega\;Df(\mu D)[\rho_m(\omega)$$
$$\times\;\Re R_0(\omega+\mu D)+\rho_0(\omega)\;\Re R_m(\omega+\mu D)], \tag{11}$$

where $\Re R_{0,m}$ denotes the real part of $R_{0,m}$. In the universal limit, in particular $T/D\to0$, so that only the terms $\propto f(-D)\approx1$ survive. Furthermore, in this limit the weighted spectral densities $e^{-\beta\omega}\rho_{0,m}(\omega)/Z_f$ contribute significantly only for frequencies less than the impurity part of the ground-state energy $E_0<0$, because $e^{\beta E_0}Z_f$ tends to 1 for low temperatures. From perturbation theory it follows[16] that $e^{-\beta\omega}\rho_f(\omega)/Z_f$ vanishes asymptotically as $1/\omega^2$ for large, negative ω. Hence it contributes significantly to the integral in Eq. (11) only for

$$-\sqrt{D}\lesssim\omega\lesssim E_0.$$

In this frequency interval, $\Re R_f(\omega-D)$ can be replaced by its bare counterpart $1/(\omega-H_f-D)\approx(-1)/D$:

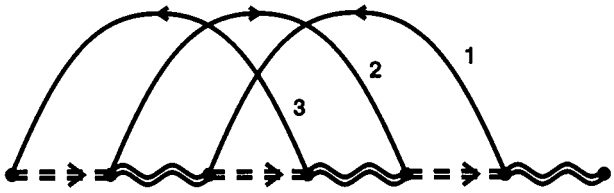

FIG. 3. Skeleton diagram of order 6 for $\Sigma_0 R_0$.

$$D\frac{\partial}{\partial D}F_f^{(2)}=\frac{-V^2\rho}{NZ_f}\sum_{m=1}^{N}\int e^{-\beta\omega}d\omega[\rho_m(\omega)+\rho_0(\omega)].$$

Together with Eq. (7), the following scaling relation is obtained:

$$D\frac{\partial}{\partial D}F_f^{(2)}=\rho V^2(1-1/N)\frac{\partial}{\partial\epsilon_f}F_f^{(2)}-\rho V^2. \tag{12}$$

This is called henceforth the second scaling equation. Next it is shown that in the universal limit all families of higher-order skeleton diagrams of Υ are *irrelevant*, by which is meant here that their contribution to the logarithmic derivative in Eq. (12) vanishes as $O(1/D)$. For the proof see Appendix A, the families of skeleton diagrams being needed to enforce the variational principle.

The result can be made plausible by casting it into the language of diagrams, as in Fig. 2. Differentiating logarithmically with respect to D means removing one curved conduction-electron line and replacing the internal propagator by its value at the cutoff $\propto 1/D$. Therefore this diagram contributes $\propto D/D$ to the logarithmic derivative.

For a diagram of higher order than two such as in Fig. 3, there lie under *each* conduction-electron line at least three propagators, because otherwise this diagram would have a self-energy insertion. Hence its contribution to the logarithmic derivative is $\propto D/D^3$, and can be neglected for large D.

Equation (12) therefore holds as well for the *exact* F_f. It describes the Haldane scaling[17] for the difference F_f-E_0; that is, it depends on D and ϵ_f only via

$$(F_f-E_0)(T,V,\rho,\epsilon_f,D)=(F_f-E_0)(T,V,\rho,\epsilon_f^*),$$

$$\epsilon_f^*=\epsilon_f+(1-1/N)\rho V^2\ln D/(\rho V^2).$$

By inserting this into Eq. (10), in the magnetic limit $-\epsilon_f\gg\rho V^2$ the scaling law

$$F_f-E_0=Tg(T,V,\epsilon_f,D,\rho)=Tg\left(\frac{T}{\Gamma},\frac{T}{T_K}\right) \tag{13}$$

follows, with the quantity $\Gamma=\pi\rho V^2/N$ and (up to a numerical factor) the Kondo temperature[2]

$$T_K=D\sqrt[N]{\rho V^2/D}\exp[\epsilon_f/\rho V^2]. \tag{14}$$

This proves the universal behavior for the free energy of the Anderson Hamiltonian, as well as that the energy scales Γ and T_K are the exact ones. In particular, it has been shown that the NCA preserves the *exact* energy scales of the system. Because the NCA is exact up to orders V^4 and $1/N$, an inclusion of families of skeleton diagrams of higher order in Eq. (13) will slightly change g but *not the energy scales*, and consequently will not alter the approximation qualitatively. Such an extension of the NCA has been performed,[18] and within the errors of the numerical calculation the scaling law (13) as well as a slight change in the respective function g have been verified.

There holds an analogy to the usual diagrammatic renormalization group, as described Sec. I. It turns out that from a certain order in perturbation theory on, the energy scales obtained by that method do not change any more in the universal limit, while, for an observable the form of its respective function g can still change. However, the point is that this scheme can only be used for high temperatures $T\gg T_K$, below which perturbation theory breaks down. Hence a necessary condition for a diagrammatic technique to describe the universal behavior of impurity systems is that it includes families of skeleton diagrams *including* those of second order. This result can straightforwardly be extended to the case of finite magnetic fields.

IV. SCALING WITH MAGNETIC FIELD

The influence of a magnetic field h on the host metal is of order $h/D\propto 1/D$, and can be neglected. Hence, to the Hamiltonian of Eq. (1), only

$$H_f\rightarrow H_f+g\mu_B h\sum_m m\ f_m^+ f_m \tag{15}$$

is added, where g denotes the g factor of the f electron, and μ_B is the Bohr magneton. The functional Υ will explicitly depend on h only via the new term in H_f. Consequently the first scaling equation (10) changes to

$$F=T\frac{\partial}{\partial T}F+\rho V^2\frac{\partial}{\partial\rho V^2}F+\epsilon_f\frac{\partial}{\partial\epsilon_f}F+g\mu_B h\frac{\partial}{\partial g\mu_B h}F$$
$$+D\frac{\partial}{\partial D}F. \tag{16}$$

The second scaling equation (12) remains unaffected. The scaling law for the magnetization $M(h)=-(\partial/\partial h)F_f$ therefore reads

$$M(T,V,\epsilon_f,D,\rho,h)=M\left(\frac{T}{\Gamma},\frac{T}{T_K},\frac{h}{\Gamma},\frac{h}{T_K}\right). \tag{17}$$

V. PROOF OF UNIVERSALITY

To obtain the scaling of any observable, the Hamiltonian H has to be coupled to suitable external fields. However, only the skeleton diagram of Fig. 2 is relevant for large D. Analogous scaling equations such as Eqs. (10) and (13) can thus be derived for any other observable, hence proving universality for the Anderson model.

As an example, take the f propagator[14] as a function of imaginary time τ,

$$G_{fm}(\tau)=-\langle T_\tau F_m(\tau)F_m^+(0)\rangle. \tag{18}$$

Here T_τ is the time-ordering operator, and $\langle\ \rangle$ denotes the thermodynamic average with respect to H. With the help of $Q(z)$ one can reproduce the well-known integral representation for G_{fm} which coincides for fermionic Matsubara frequencies with the Fourier transform of $G_{fm}(\tau)$,[19]

$$G_{fm}(\omega)=\oint e^{-\beta z}\frac{dz}{2\pi i}\langle\langle 0|Q(z)|0\rangle\langle m|Q(z+\omega)|m\rangle\rangle_c .$$

To obtain a variational functional for G_{fm}, H is coupled to an auxiliary fermionic field Ψ:

$$H+\omega\Psi^+\Psi+V\sqrt{\rho}\lambda(\Psi^+ b^+ f_m+\text{H.c.}).$$

The f propagator is obtained from all diagrams of second order in λ that is, after removing the Ψ propagator.[10] A functional Υ_Ψ can be constructed analogously to Eq. (5), to give, at the saddle point,

$$Z_\Psi:=\frac{\mathrm{Tr}_f\mathrm{Tr}_c\mathrm{Tr}_\Psi e^{-\beta H}}{\mathrm{Tr}_c\mathrm{Tr}_\Psi e^{-\beta(H_c+H_\Psi)}}.$$

G_f follows as

$$\left.\frac{\partial}{\partial\lambda^2}\right|_{\lambda=0} F_\Psi=\rho V^2 f(\omega)G_{fm}(\omega). \tag{19}$$

The scaling equations for F_Ψ, and via Eq. (19) for G_f, can be established in the same manner as for F_f. In particular, Eq. (10) now reads

$$\left(T\frac{\partial}{\partial T}+\omega\frac{\partial}{\partial\omega}+\epsilon_f\frac{\partial}{\partial\epsilon_f}+\rho V^2\frac{\partial}{\partial\rho V^2}+D\frac{\partial}{\partial D}+1\right)G_{fm}=0. \tag{20}$$

In the universal limit of large D, again only the *skeleton diagrams of second order* are relevant, and the analog to Eq. (12) holds for G_f, too:

$$D\frac{\partial}{\partial D}G_{fm}=\rho V^2(1-1/N)\frac{\partial}{\partial\epsilon_f}G_{fm}.$$

In the magnetic limit $-\epsilon_f\gg\Gamma$, where $\Gamma\gg T_K$, it follows that the Abrikosov-Suhl resonance and the impurity part of the resistivity computed within the NCA scale with the exact Kondo temperature. This was numerically observed in Ref. 20. There, the energy scale was determined as the maximum value of the spectral density of $G_{fm}(\omega)$ in the magnetic limit of the Anderson model, and *assumed* to be proportional to T_K. Here this has been proved.

VI. DESCRIPTION OF CROSSOVER: WILSON NUMBER

Within this scaling method the crossover phenomenon[6] can now be described entirely within a diagrammatic approach. Even for the skeleton diagrams of second order, an analytical solution of the self-consistency equations does not seem possible for finite temperature. However, for zero temperature the well-known expressions for the ground-state energy of the NCA[10,21] for the Anderson model can be evaluated analytically (see Appendix B) in the magnetic limit. In this limit, it follows from Eq. (17) that for zero temperature the scaling law

$$M(V,\epsilon_f,D,\rho,h)=M\left(\frac{h}{T_K}\right) \tag{21}$$

holds, which holds as well for the NCA, as shown above. For low magnetic fields, the low-field energy scale T_L can be fixed unambiguously by the static magnetic susceptibility at vanishing magnetic field[2],

$$\chi(0)=\tfrac{1}{3}\mu_j^2/T_L .$$

With the help of the analytical NCA results of Appendix B, an *analytical* expression for T_L is obtained:

$$T_L^{\mathrm{NCA}}=T_K/\Gamma(1-1/N), \tag{22}$$

with Γ being the gamma function. The result coincides up to order $1/N$ with the result $T_L=T_K\Gamma(1+1/N)$, which is believed to be exact.[2]

For high magnetic fields $g\mu_B h\gg T_K$, the NCA reproduces the perturbation theory up to V^4. With the definitions $N=2j+1$ and $J=V^2/|\epsilon_f|$, for the impurity part of the magnetization the expansion

$$\frac{M(h)}{jg\mu_B}=1-\frac{\rho J}{N}+\frac{(\rho J)^2}{N}\ln\frac{g\mu_B h\sqrt[N]{e}}{D\sqrt[N]{\epsilon_f/D}}+\frac{(\rho J)^2}{N}\left[\frac{2}{N(N-1)}\sum_{m=1}^{N-1} m\ \ln(m)\right]+O(J^3)$$

is obtained. The exact scaling (21) of the NCA renders it possible to reexpress in the perturbation expansion J in terms of h/T_K. The high-field energy scale T_H is fixed unambiguously[2] by requiring that terms $\propto 1/\ln^2[g\mu_B h/T_H]$ be absent in the resulting asymptotic expansion. One arrives at the well-known asymptotic renormalization-group result for the magnetization in high magnetic fields,

$$\frac{M(h)}{jg\mu_B}=1-\frac{1}{N}\frac{1}{\ln\frac{g\mu_B h}{T_H}}-\frac{1}{N^2}\frac{\ln\ln\frac{g\mu_B h}{T_H}}{\ln^2\frac{g\mu_B h}{T_H}}+O\left(\frac{\ln\ln\frac{g\mu_B h}{T_H}}{\ln^3\frac{g\mu_B h}{T_H}}\right), \tag{23}$$

and T_H is given by

$$T_H=T_K\exp\left[-1/N-\frac{2}{N(N-1)}\sum_{m=1}^{N-1} m\ln(m)\right]. \tag{24}$$

The Wilson number $W=T_H/T_L$ characterizes the crossover from the high-field region, where the impurity reacts as an asymptotically free magnetic moment, to the low-energy region where the impurity is screened. Hence the Wilson number coincides with the exact result up to order $1/N$:

$$\frac{W^{\mathrm{NCA}}}{W}=\frac{1}{\Gamma(1-1/N)\Gamma(1+1/N)}=1+O(1/N^2). \tag{25}$$

By a Schrieffer-Wolff transformation,[14] this result can be extended to the Coqblin-Schrieffer model (see Appendix C).

VII. HOW MUCH DOES SCALING DEPEND ON BAND STRUCTURE?

The universal behavior of impurity models like the Anderson model should not depend on details of the host's density of states as long as its band has a finite density of states at the Fermi energy.[3] This was realized for model (1) by assuming a constant density of states with a sharp cutoff at $\pm D$, as the other approaches to scaling do.[2,3,8] There it is assumed that the energy scales of the system do not change as long as the density of states is finite at the Fermi energy, and scales as $\tilde{\rho}(\epsilon)=\rho(\epsilon/D)$, which means that the band is sufficient structureless to have only one energy scale D.

Here this is proved: The first scaling equation (10) can be taken over because of

$$T\frac{\partial}{\partial T}\rho(\epsilon T/D)=-D\frac{\partial}{\partial D}\rho(\epsilon T/D).$$

For the second scaling equation (12), the term

$$Y:=V^2\int_{-\infty}^{\infty}\rho(\epsilon/D)\Lambda_2(\omega+\epsilon)f(\epsilon)d\epsilon$$

as in Eq. (A2) in Appendix A is examined, which represents an integration over a conduction-electron line. Λ_2 stands for the real part of the m propagators which lie under this conduction-electron line. Differentiating logarithmically with respect to D and substituting $\epsilon:=uD$ yields

$$D\frac{\partial}{\partial D}Y=(-D)\int_{-\infty}^{\infty}u\rho'(u)f(uD)\Lambda_2(\omega+uD)\,du.$$

The integrand can be neglected outside the interval $-\sqrt{D}\lesssim\omega\lesssim 0$ as in Sec. III B. If ρ is sufficiently smooth around the Fermi energy, the integrand contributes significantly only for $-1\lesssim u\lesssim 1/\sqrt{D}$. Therefore one can replace $\Lambda_2(\omega+uD)$ by its asymptotic value $1/(-uD)^m$, and the Fermi function by its $T=0$ values up to terms of order $1/D$. Y scales as

$$D\frac{\partial}{\partial D}Y\propto D^{1-m}.$$

Only the skeleton diagrams of second order ($m=1$) are relevant,

$$D\frac{\partial}{\partial D}Y\propto V^2\int_{-\infty}^{0}\rho'(u)du=V^2\rho(0).$$

Thus the second scaling equation is still valid, and depends on the density of states only through its value at the Fermi energy.

Magnetic impurity in a superconductor

If the density of states of the host has still one energy scale D, but the density at the Fermi surface vanishes according to a power law, this models magnetic impurities in superconductors[22] with gap nodes:

$$\rho(\omega)=(1+r)\overline{\rho}\left(\frac{\omega}{D}\right)^r,\qquad \int_{-D}^{D}\rho(\omega)d\omega=2D\overline{\rho}. \tag{26}$$

This modifies the scaling law (12) accordingly: Every skeleton diagram depends explicitly on D via the integration boundaries, which sorts out the NCA diagrams as the only relevant diagrams. In addition, every skeleton diagram has one factor D^{-r} per loop. Hence the second scaling equation is

$$D\frac{\partial}{\partial D}F_f=(1+r)(1-1/N)\overline{\rho V}^2\frac{\partial}{\partial\epsilon_f}F_f-r\overline{\rho V}^2\frac{\partial}{\partial\overline{\rho V}^2}F_f-(1+r)\overline{\rho V}^2. \tag{27}$$

The first scaling equation remains unchanged. In the limit of large N, this scaling equation is consistent with the results of Fradkin,[23]

$$T_K=D\left(1-\frac{r}{(1+r)J\overline{\rho}}\right)^{1/r}. \tag{28}$$

VIII. ALTERNATIVE DIAGRAMMATIC METHODS

What conclusions can be drawn from this theory as to the reliability of other diagrammatic approaches, especially their ability to describe the crossover?

A. NCA and the 1/N expansion

If the system has N internal degrees of freedom and exhibits local Fermi-liquid behavior, the $1/N$ expansion becomes exact in the limit of large N.[24] Contrary to common belief,[2,25] the $1/N$ expansion is *not* suited for the perturbative regime of high temperatures or magnetic fields because it fails to reproduce the diagrammatic renormalization-group results. That is so because the Kondo temperature itself is a function of $1/N$. Hence it is not possible to describe the *crossover* within a finite-order $1/N$ expansion.

The NCA was considered so far as a ''self-consistent'' $1/N$ expansion.[14,25] However, this does not explain why the NCA values for the static magnetic susceptibility relative to their $T=0$ value agree so well with the respective renormalization-group results,[26] even for $N=2$. In view of Eq. (17), this now becomes clear.

B. Higher order skeleton diagrams

One may ask whether it is possible to improve the NCA substantially by incorporating in Υ skeleton diagrams of higher order. However, one has to be aware that then the numerical problems in solving the self-consistency equations become formidable.[18] To date one has not succeeded to calculate $\chi(0)$, and hence the Wilson number up to order $1/N^2$ by this diagrammatic approach.

C. Non-self-consistent methods

One way of incorporating higher-order skeleton diagrams in a theory for impurity systems was put forward by Saso[27] in his T-matrix approach. The impurity propagators R_f were calculated within the NCA. For an observable, these NCA propagators were inserted into the respective skeleton diagrams of orders higher than 2. Such an approach cannot be derived from a variational principal. Hence it will not correctly describe the universal behavior of the impurity.

D. Coleman's diagram technique

In Coleman's approach[12] to the Hamiltonian (1), the constraint $n_f+n_b=1$ is enforced by adding $\lambda(n_f+n_b)$ to H and sending λ to infinity; consequently, H_f in Eq. (1) changes to

$$H_f=(\epsilon_f+\lambda)\sum_m f_m^+ f_m+\lambda b^+ b. \tag{29}$$

The scaling equations (10) and (12) are rederived with the help of this diagram technique, and then Coleman's technique is used to discuss the conserving slave-boson approach by Kroha *et al.*[28]

Now that the unperturbed part H_c+H_f is a one-particle Hamiltonian, the standard Matsubara-perturbation theory can be developed. The naked propagators from which the diagram technique is built are given by

$$\begin{aligned} R_m^{(0)}(i\omega_n)&=1/(i\omega_n-\epsilon_f-\lambda),\\ R_0^{(0)}(i\omega_n)&=1/(i\nu_p-\lambda),\\ R_{cm}^{(0)}(i\omega_n)&=\rho\int_{-D}^{D}\frac{1}{i\omega_n-\epsilon}d\epsilon. \end{aligned} \tag{30}$$

Here $i\omega_n=2\pi(n+1/2)T$ and $i\nu_p=2\pi nT$ are the fermionic and bosonic Matsubara frequencies, respectively. The vertices are displayed in Fig. 1. Again, a dashed line denotes $R_m^{(0)}$, a wavy line $R_0^{(0)}$, and a solid line represent the propagator of a conduction electron $R_{cm}^{(0)}$. This propagator already contains the sum over all momenta because of the local interaction with the impurity.

Skeleton diagrams can be defined as above as containing no self-energy insertions. The variational principle follows with the help of the functional

$$\begin{aligned} -\frac{\tilde{\Upsilon}}{T}:=&\sum_{m,n,v}\left(3-\frac{2}{v}\right)\Sigma_m^{(v)}(i\omega_n)R_m(i\omega_n)+\sum_{mn}[\ln(i\omega_n-\epsilon_f\\ &-\lambda-\Sigma_m(i\omega_n))-\ln(i\omega_n-\epsilon_f-\lambda)]\\ &+\sum_{mn}\{\ln([R_{cm}^{(0)}]^{-1}-\Sigma_{cm}(i\omega_n))-\ln[R_{cm}^{(0)}]^{-1}\}\\ &-\sum_{p,v}\left[\ln(i\nu_p-\lambda-\Sigma_0(i\nu_p))-\sum_p\ln(i\nu_p-\lambda)\right]. \end{aligned} \tag{31}$$

The factor $3-2/v$ arises because every term $\Sigma^{(v)}R$ contains $3v/2$ propagators. It is straightforward to show that $\tilde{\Upsilon}$ is stationary with respect to variations of the propagators if the Dyson equations hold. By rearranging the internal summation frequencies, one has the following identity:

$$\begin{aligned} \sum_{m,n}\Sigma_m(i\omega_n)R_m(i\omega_n)&=\sum_{m,n}\Sigma_{cm}(i\omega_n)R_{cm}(i\omega_n)\\ &=(-1)\sum_p\Sigma_0(i\nu_p)R_0(i\nu_p), \end{aligned} \tag{32}$$

the minus sign in the second line coming from the additional fermion loop.[12]

As in Luttinger's original approach,[9] one shows that $\tilde{\Upsilon}$ is equal to the difference of the interacting and noninteracting free energy F:

$$\tilde{\Upsilon}=F(V)-F(0)=:\Delta F. \tag{33}$$

The Hilbert space is a sum of eigenspaces of the number operator $n=\Sigma_m f_m^+ f_m+b^+ b$. The partition function can then be represented as a sum over these subspaces. The subspace $n=0$ describes the noninteracting system. In Coleman's original approach, the physical subspace $n=1$ is projected out by

$$\lim_{\lambda\to\infty}\frac{\partial}{\partial e^{-\beta\lambda}}\frac{-\Delta F}{T}=\lim_{\lambda\to\infty}Z_f(\lambda)=Z_f. \tag{34}$$

The limit is approached smoothly so that

$$\lim_{\lambda\to\infty}\frac{\partial}{\partial\lambda}Z_f(\lambda)=0. \tag{35}$$

1. First scaling equation

Analogously to Sec. III A, the explicit derivatives with respect to ρV^2, ϵ_f, and λ are

$$\rho V^2\frac{\partial}{\partial\rho V^2}\frac{\Delta F}{T}=\sum_{m,n,v}[\Sigma_m^{(v)}(i\omega_n)R_m(i\omega_n)], \tag{36}$$

$$\frac{\partial}{\partial\epsilon_f}\frac{\Delta F}{T}=\sum_{m,n}R_m(i\omega_n), \tag{37}$$

$$\frac{\partial}{\partial\lambda}\frac{\Delta F}{T}=\sum_{m,n}R_m(i\omega_n)-\sum_p R_0(i\nu_p). \tag{38}$$

To determine the T dependence of $\tilde{\Upsilon}$, one has to bear in mind that each Matsubara frequency is proportional to T, that each summation over Matsubara frequencies gives a factor T, and that in a diagram of order v there are $v/2$ such summations. Furthermore, $R_{cm}^{(0)}$ depends on T and D only via D/T. Together with Eqs. (32), (36), (37), and (38), it follows that

$$\Delta F=\left(T\frac{\partial}{\partial T}+\epsilon_f\frac{\partial}{\partial\epsilon_f}+\rho V^2\frac{\partial}{\partial\rho V^2}+\lambda\frac{\partial}{\partial\lambda}+D\frac{\partial}{\partial D}\right)\Delta F. \tag{39}$$

By using Eqs. (34) and (35), the analog of the scaling equation (10) follows:

$$\left(T\frac{\partial}{\partial T}+\epsilon_f\frac{\partial}{\partial \epsilon_f}+\rho V^2\frac{\partial}{\partial \rho V^2}+D\frac{\partial}{\partial D}\right) Z_f=0. \tag{40}$$

2. Second scaling equation

The functional $\tilde{\Upsilon}$ depends on the cutoff D only via the integration boundaries $\pm D$ in $R_{cm}^{(0)}$. Hence

$$D\frac{\partial}{\partial D}\frac{\Delta F}{T}=\sum_{mn}\,[R_{cm}^{(0)}(i\omega_n)]^{(-2)}\left(\frac{D}{i\omega_n+D}+\frac{D}{i\omega_n-D}\right)\times[R_{cm}(i\omega_n)-R_{cm}^{(0)}(i\omega_n)]. \tag{41}$$

The propagator difference $R_{cm}-R_{cm}^{(0)}$ can be expanded as

$$Y:=(R_{cm}-R_{cm}^{(0)})[R_{cm}^{(0)}]^{(-2)}=\Sigma_{cm}+\Sigma_{cm}R_{cm}^{(0)}\Sigma_{cm}+\cdots. \tag{42}$$

In either case discussed below, it will turn out that only the second-order term

$$\Sigma_{cm}^{(2)}(i\omega_n)=\frac{V^2\rho T}{N}\sum_p\,R_m(i\omega_n+i\nu_p)R_0(i\nu_p)$$

is relevant in the universal limit of large D. The propagators $R_{0,m}$ have the spectral decomposition

$$R_{0,m}(z)=\int\frac{dx}{z-x-\lambda}\rho_{0,m}(x), \tag{43}$$

and are centered[12] around λ. After performing Matsubara summations, this gives

$$D\frac{\partial}{\partial D}\frac{\Delta F^{(2)}}{T}=\frac{V^2\rho}{N}D\beta\sum_{m,\sigma=\pm1}\int\int dx\;dy\;\rho_m(x)\rho_0(y)\times\frac{[f(x+\lambda)+b(y+\lambda)][f(\sigma D)-f(x-y)]}{\sigma D-x+y}, \tag{44}$$

with f and b the Fermi and Bose functions, respectively. The coefficient of $e^{-\beta\lambda}$ in Eq. (44) for large D, when combined with Eqs. (37) and (38), yields, because of Eq. (34), the desired scaling equation (13).

In Eq. (42) higher-order terms in Σ are of higher order in $e^{-\beta\lambda}$, and vanish relatively to Σ_{cm} in the limit of large λ. By the same arguments as given in Sec. III B, one can show that skeleton diagrams of higher order in Σ_{cm} are irrelevant: Higher-order skeleton diagrams in Eq. (42) contain at least three impurity propagators which have to be evaluated at $i\omega_n=\pm D$ to make a contribution $\propto 1/D^2$, or they are of higher order in $e^{-\beta\lambda}$.

E. Conserving slave-boson approach

Kroha *et al.*[28] developed, for the Anderson model, a method quite similar to the NCA. It is constructed from skeleton diagrams within Coleman's slave-boson technique. Kroha *et al.*, however, imposed the constraint only in the average $\langle n_f+n_b\rangle_H=1$. Their method then does not violate the gauge symmetries of the model like the usual slave-boson mean-field approach.[28] The boundary condition for the free energy is

$$\frac{\partial}{\partial\lambda}F=\langle n_f+n_b\rangle_H=1. \tag{45}$$

This includes unphysical states. Consequently, the conduction electrons acquire a self-energy. The first scaling equation (39) now reads

$$\Delta F=\left(T\frac{\partial}{\partial T}+\epsilon_f\frac{\partial}{\partial\epsilon_f}+\rho V^2\frac{\partial}{\partial\rho V^2}+D\frac{\partial}{\partial D}\right)\Delta F+\lambda-\lambda\,\frac{\partial}{\partial\lambda}\,F(0). \tag{46}$$

In order to obtain any *observable*, ΔF has to be differentiated once more with respect to an external field. Hence this equation is the analog to Eq. (10).

The second scaling equation can be derived from Eq. (44) in the limit of large D. First it is summed over σ. Only the term $\propto f(\sigma D)$ survives, because the propagators R have a spectral weight centered around a *finite* value of λ, and $\Sigma_\sigma\lim_{D\to\infty}D/(\sigma D-x+y)=0$. With Eqs. (37), (38), and (45), one has

$$D\frac{\partial}{\partial D}\frac{\Delta F^{(2)}}{T}=\frac{-V^2\rho\beta}{N}\sum_m\int\int dx\;dy\;\rho_m(x)\rho_0(y)\times[f(x+\lambda)+b(y+\lambda)]=(1-1/N)V^2\rho\frac{\partial}{\partial\epsilon_f}\frac{\Delta F^{(2)}}{T}-V^2\rho\beta.$$

More generally, because $\Sigma_\sigma\lim_{D\to\infty}D/(i\omega_n+\sigma D)=0$ in every propagator of Eq. (41) the Matsubara frequency $i\omega_n$ can be replaced by σD with an overall factor $f(\sigma D)$. In the magnetic limit one has $\lambda\gtrsim|\epsilon_f|$ to enforce[28] both $n_f\approx1$ and $n_b\approx0$. Therefore higher-order terms in Eq. (42) are irrelevant, because they are either $o(1/D)$, or of higher order in $e^{-\beta\lambda}$.

Hence the approximation also preserves the exact scaling laws. This explains why their results for the f propagator are so similar to the respective NCA results.[14] Moreover, one can now predict that taking into account more skeleton diagrams will not alter the picture qualitatively.

IX. SUMMARY

The Anderson-impurity model shows, in a nutshell, the difficulties when dealing with strong correlations. One encounters the same problems as in high-energy physics: the perturbation theory of observables at energies T in the coupling constant diverges logarithmically, $\propto\ln D/T$. The limit of zero energy T in solid-state physics corresponds to the limit of infinite cutoff D in high-energy physics. If the Hamiltonian can be shown to be renormalizable, it means that there are finitely many energy scales in the system, at least in the perturbative region. If there is but one scale, the system can be described by a ''running'' coupling constant $J(D)$, expressed with the help of the β function

$$\beta(J)=\frac{d\;J(D)}{d\;\ln D}. \tag{47}$$

Reducing the cutoff D of the system does not change its physics as long as the effective coupling $J(D)$ is changed according to Eq. (47), to keep the energy scale constant.

However, outside the energy regime where the perturbation theory is valid it has never been shown that such a β function exists at all.

In this paper, the variational functional of Luttinger and Ward was used to prove both the *existence* and *form* of the β function, or, in other words, the exact energy scales of an impurity system were determined. It turned out that neglecting the vertex corrections (NCA) suffices to prove universal behavior, and that families of higher-order skeleton diagrams do *not* alter the energy scales.

The method differs therefore from the conventional renormalization-group approach. Within that approach, the fixed points of a flow of effective Hamiltonians is studied perturbatively as the energy scales of the system are varied. The crossover is inaccessible by that method.

In comparison to that, the skeleton diagrams can describe the crossover very well, as was demonstrated. However, the theory cannot predict the nature of the fixed-point Hamiltonian.

Further work on this subject will concentrate on the question of whether the NCA can also be justified as a means to solve the effective impurity model onto which the infinite-dimensional versions of correlated electron systems can be mapped.[29,30] In particular, one would like to learn whether the periodic Anderson Hamiltonian exhibits heavy fermion behavior in this limit, or if this is only an artifact of the approximations used. Also, it should be within the reach of the theory to decide which class of diagrams should be used to describe the problem of two impurities in a metal.

ACKNOWLEDGMENTS

It was a pleasure to discuss the intricacies of diagrammatic approaches with Tom Schork and Professor V. Zevin. I would like to thank Professor P. Fulde and G. Zwicknagl for suggesting that I investigate the NCA, and for their constant interest in the progress of this work.

APPENDIX A: IRRELEVANCE OF HIGHER-ORDER SKELETON DIAGRAMS

The proof uses the spectral decomposition of the ionic propagators R_f. Every skeleton diagram depends explicitly on D only via the integration boundaries $\pm D$ coming from integration over the conduction-electron lines, as shown in Eq. (6). For $\alpha=0,\ldots,N$, let $\Sigma_\alpha^{(2n)}R_\alpha$ be such a skeleton diagram of $2n$th order with p closed fermion loops and n ionic propagators R_i:

$$\oint\frac{dz}{2\pi i}e^{-\beta z}\Sigma_\alpha^{(2n)}(z)R_\alpha(z)$$
$$=\frac{\rho^n V^{2n}}{N^{n-p}}\oint\frac{dz}{2\pi i}$$
$$\times e^{-\beta z}\prod_{j=1}^{n}\int_{-D}^{D}f(\epsilon_j)d\epsilon_j\prod_{i=1}^{n}R_i\left(z+\sum_j^{(i)}\epsilon_j\right). \tag{A1}$$

Here $\int d\epsilon_j$ denotes the integration over the jth conduction-electron line. Furthermore, the term $\Sigma_j^{(i)}$ in the argument of R_i indicates that the sum runs over j if the ith propagator sits under the jth conduction-electron line, as in Fig. 3, the numbers indicating the ϵ_j. The ith propagator R_i of the respective skeleton diagram has the spectral decomposition

$$R_i\left(z+\sum_j^{(i)}\epsilon_j\right)=\int_{-\infty}^{\infty}d\lambda_i\rho_i(\lambda_i)\Big/\left(z+\sum_j^{(i)}\epsilon_j-\lambda_i\right).$$

For that reason, the line integral gives only contributions from the real poles,

$$z=\omega_k=\lambda_k-\sum_j^{(k)}\epsilon_j.$$

For real ω, there holds the relation

$$\Re R_{0,m}(\omega)=\int_{-\infty}^{\infty}\frac{\rho_{0,m}(\lambda)}{\omega-\lambda}d\lambda,$$

where the Cauchy-principal value of the integral has to be taken. Hence the kth pole of the line integrals gives

$$\prod_{j=1}^{n}\int_{-D}^{D}f(\epsilon_j)d\epsilon_j\int_{-\infty}^{\infty}d\omega\ e^{-\beta\left(\omega-\Sigma_j^{(k)}\epsilon_j\right)}\rho_k(\omega)$$
$$\times\prod_{i\neq k}^{n}\Re R_i\left(\omega-\sum_j^{(k)}\epsilon_j+\sum_j^{(i)}\epsilon_j\right).$$

Because of $f(\epsilon_j)e^{\beta\epsilon_j}=f(-\epsilon_j)$, one shifts those variables ϵ_j to $-\epsilon_j$, which occur in $\Sigma^{(k)}$ but not in $\Sigma^{(i)}$:

$$\prod_{j=1}^{n}\int_{-D}^{D}f(\epsilon_j)d\epsilon_j\int_{-\infty}^{\infty}d\omega\ e^{-\beta\omega}\rho_k(\omega)\prod_{i\neq k}^{n}\Re R_i\left(\omega+\sum_j^{(i)}\epsilon_j\right),$$

where now $\Sigma_j^{(i)}$ runs over j if the propagator R_i sits under the jth conduction-electron line in the respective skeleton diagram with cyclic permutated vertices. In such a diagram, the propagator R_k is the outer one.

Exactly *here* one uses the fact that only whole families of skeleton diagrams are considered: It was just shown that for every family F of $2n$th-order skeleton diagrams their contribution to the line integral in Eq. (5) is

$$\mathrm{Tr}_f\oint\frac{dz}{2\pi i}e^{-\beta z}\Sigma_f^{(2n,F)}(z)R_f(z)$$
$$=2n\int d\omega\ e^{-\beta\omega}\times\Big[\rho_0(\omega)\mathrm{Re}\Sigma_0^{(2n,F)}(\omega)$$
$$+\sum_m\rho_m(\omega)\mathrm{Re}\Sigma_m^{(2n,F)}(\omega)\Big].$$

Here, the operator Re is defined to replace *every* propagator in its argument by its real part. The factor $2n$ arises because every skeleton diagram occurs in a family $2n$ times. In Υ, every skeleton diagram of order $2n$ depends explicitly on D only via the integration boundaries $\pm D$ of its n integrations over the conduction-electron lines. The ith integral over a conduction-electron line can be written as

$$\mathrm{Re}\Sigma_f^{(2n,F)}(\omega)=\left(\int_{-D}^{D}\right)^{n-1}\Lambda_1(\omega)\int_{-D}^{D}d\epsilon_i f(\epsilon_i)\Lambda_2(\omega+\epsilon_i), \tag{A2}$$

where the part Λ_1 of the respective diagram does not depend on ϵ_i; that is, its ionic propagators are lying on the left or the right of the ith conduction-electron line. The propagators of part Λ_2 lie under the ith conduction-electron line. $(\int)^{n-1}$ hints at the other $n-1$ integrations, weighted with the respective Fermi functions. One differentiates with respect to D by evaluating the integral over the ith conduction-electron line ϵ_i at its integration boundaries $\pm D$,

$$2n \sum_{\sigma=\pm 1} \int d\omega\, e^{-\beta\omega} \rho_{0,m}(\omega) \times [\Lambda_1(\omega) D f(\sigma D) \Lambda_2(\omega+\sigma D)].$$

The integral is to be weighted with $1/Z_f$ in order to yield the D derivative of the respective contribution to the free energy. Because $e^{\beta E_0} Z_f$ goes for low temperatures to 1, the spectral densities $\rho_{0,m}$ are weighted with $e^{\beta(E_0-\omega)}$. For low temperatures $T \ll D$, this weighted spectral density contributes to the integral only for frequencies $\omega \lesssim E_0$. Because the other integrations over conduction-electron lines ϵ_j are weighted with Fermi functions $f(\epsilon_j)$, respectively, for low temperatures $T \ll D$ the real part of a propagator $\Re R_f(\omega - D + \Sigma_j \epsilon_j)$ contributes in $\Lambda_2(\omega - D)$ only for frequencies

$$\omega - D \lesssim E_0 - D < -D.$$

In this frequency interval one can replace $\Re R_f$ by its naked counterpart $1/(\omega - H_f - D)$, and hence can estimate its contribution to F_f from above as $1/D$. The term $\propto f(D)$ does not contribute for $T \ll D$. It therefore can be estimated as

$$\frac{1}{Z} D \frac{\partial}{\partial D} \Sigma_f^{(2n)} R_f \propto D/D^{m_i}.$$

Hence at least one m_i must equal 1, otherwise the skeleton diagram is irrelevant. However, such a diagram is a skeleton *only* if it is of second order; otherwise it would have a self-energy insertion. Equation (12) follows.

APPENDIX B: NCA AT ZERO TEMPERATURE

1. NCA differential equations

The NCA equations (6) together with the Dyson equations (4) constitute a self-consistent system of equations which have been solved numerically.[20] For $T=0$ the NCA integral equations (6) in a magnetic field are transformed into differential equations by substituting for the Fermi function a step function,[21,16,14] by introducing the negative, inverse of the propagators $R_{0,m}$,

$$Y_0(z) = \Sigma_0^{(2)}(z) - z,$$

$$Y_m(z) = \Sigma_m^{(2)}(z) + \epsilon_f - z, \tag{B1}$$

and $Y_m = \overline{Y_m} + mg\mu_B h$ for $-j \leq m \leq j = (N-1)/2$,

$$\frac{\partial}{\partial \omega} Y_0 = -1 - \frac{\rho V^2}{N} \sum_m \frac{1}{\overline{Y_m} + mg\mu_B h},$$

$$\frac{\partial}{\partial \omega} \overline{Y_m} = -1 - \frac{\rho V^2}{N} Y_0^{-1}. \tag{B2}$$

The inverse propagators have the asymptotic forms

$$\overline{Y_m}(\omega) \approx -\omega + \epsilon_f,$$

$$Y_0(\omega) \approx -\omega \tag{B3}$$

for large, negative ω. The NCA differential equations have, up to terms of order $O(1/D)$, the integral

$$\frac{Y_0}{\rho V^2} + \frac{1}{N} \ln \left| \frac{Y_0}{\rho V^2} \right| = \frac{\overline{Y_m}}{\rho V^2} + \frac{1}{N} \sum_m \ln \left| \frac{\overline{Y_m} + mg\mu_B h}{\rho V^2} \right| - \frac{\epsilon_f^*}{\rho V^2},$$

$$\epsilon_f^* = \epsilon_f + \left(1 - \frac{1}{N}\right) \rho V^2 \ln \frac{D}{\rho V^2}. \tag{B4}$$

The value of ϵ_f^* follows by inserting Eq. (B3). Terms of order $O(1/D)$ are neglected because the universal behavior of the system is investigated. The integral of the NCA differential equations contains the energy scales ρV^2 and T_K via[21] $\ln(T_K/\rho V^2) = \epsilon_f^*/\rho V^2$. It is a nontrivial task to solve this differential equations numerically in the universal, magnetic limit

$$D \to \infty, \quad \epsilon_f \to -\infty,$$

$$\lim_{D\to\infty} \frac{\epsilon_f}{D} = 0, \quad \frac{V^2}{|\epsilon_f|} = J = \text{const.}$$

2. What is the ground-state energy of the NCA?

The ground-state energy of the NCA is defined as

$$E_0^{\mathrm{NCA}} = \lim_{T\to 0} F_f^{\mathrm{NCA}}. \tag{B5}$$

However, one has not yet succeeded in deriving an expression for E_0^{NCA} via that route, but merely solves the NCA differential equations (B2). It has been conjectured[14] that the lowest, real zeros of the inverse propagators $Y_{0,m}$ define the NCA ground-state energy. This is now proved: Because of Eq. (B5), E_0^{NCA} fulfills

$$1 = \lim_{T\to 0} e^{\beta E_0^{\mathrm{NCA}}} \int e^{-\beta\omega} \left[\rho_0^{\mathrm{NCA}}(\omega) + \sum_m \rho_m^{\mathrm{NCA}}(\omega) \right] d\omega.$$

Hence, for $T=0$, there exist the (positive) spectral densities

$$\hat{\rho}_{0,m}^{\mathrm{NCA}}(\omega) = e^{\beta(E_0^{\mathrm{NCA}} - \omega)} \rho_{0,m}^{\mathrm{NCA}}(\omega), \tag{B6}$$

and therefore the spectral densities $\rho_{0,m}^{\mathrm{NCA}}$ vanish for $T=0$ and $\omega < E_0^{\mathrm{NCA}}$. This means that the inverse propagators $Y_{0,m}$ are real for those frequencies. In addition, $\hat{\rho}_{0,m}^{\mathrm{NCA}}$ vanish for $\omega > E_0$, because $\rho_{0,m}^{\mathrm{NCA}}$ remain finite. However, from the existence theorem for solutions of the differential equations (B2), it follows that there exists at least one value ω_0 such that the following hold.

(1) $Y_{0,m}$ have a zero in ω_0 and become complex above, if they are real for large, negative ω—which they are in view

of Eq. (B3). Because it was just shown that the $Y_{0,m}$ are real for $\omega<E_0^{\mathrm{NCA}}$, they are real for $\omega<\omega_0$ as well.

(2) $\rho_{0,m}^{\mathrm{NCA}}$ vanish for $\omega<\omega_0$; therefore $\omega_0\leqslant E_0^{\mathrm{NCA}}$.

(3) $\hat{\rho}_{0,m}^{\mathrm{NCA}}$ vanish for $\omega>\omega_0$; therefore $\omega_0\geqslant E_0^{\mathrm{NCA}}$.

To sum up: ω_0 is the lowest common zero for $Y_{0,m}$, and at the same time the NCA ground-state energy.

3. Parametrization of the NCA ground-state energy

Hence the well-known expression for the common zero of $Y_{0,m}$[21,16,31,32] can be used as the NCA ground-state energy, and is parametrized in the following manner: Define the W function for positive x as

$$W(x)\exp[W(x)]=x \qquad \text{for} \quad x\geqslant 0, \tag{B7}$$

with asymptotic behavior

$$W(x)=x+o(x^2) \qquad \text{for} \quad x\to 0^+,$$

$$W[\exp(x)]=x-\ln(x)+o(1) \quad \text{for} \quad x\to\infty. \tag{B8}$$

The integral (B4) can be solved for Y_0 because both Y_0 and Y_m are positive for $\omega<E_0^{\mathrm{NCA}}$:

$$NV^{-2}Y_0=W\left(N\exp\left[(\overline{Y_m}-\epsilon_f^*)\frac{N}{\rho V^2}+\sum_m \ln\frac{\overline{Y_m}+mg\mu_B h}{\rho V^2}\right]\right). \tag{B9}$$

E_0^{NCA} can now be parametrized with the help of

$$E_0=D+\int_{-D}^{E_0}d\omega=D+\int_{\overline{Y_m}(-D)}^{jg\mu_B h}\frac{d\omega}{d\overline{Y_m}}d\overline{Y_m},$$

the NCA differential equations (B2), and Eq. (B9) as

$$E_0=\epsilon_f-jg\mu_B h-\int_{jg\mu_B h}^{D+\epsilon_f}d\omega \times\frac{1}{1+W\left(N\exp\left[(\omega-\epsilon_f^*)\frac{N}{\rho V^2}+\sum_m \ln\frac{\omega+mg\mu_B h}{\rho V^2}\right]\right)}. \tag{B10}$$

For vanishing magnetic field there exists another parametrization, because Y_m can be written as a function of Y_0 with the help of the W function:

$$E_0=-\int_0^D\frac{d\omega}{1+W\left(\exp\left[(\omega+\epsilon_f^*)\frac{1}{\rho V^2}+\frac{1}{N}\ln\frac{\omega}{\rho V^2}\right]\right)}. \tag{B11}$$

The NCA ground-state energy fulfills Eqs. (10) and (12), as can be checked with the help of Eq. (B11). The ground-state energy is *not* a universal function because of the constant term $-\rho V^2$ in Eq. (12). The ground-state energy up to order $1/N$ and $1/D$ follows as[2]

$$E_0=\epsilon_f+\rho V^2 W\left[\frac{D}{\rho V^2}\exp\left(\frac{\epsilon_f}{\rho V^2}\right)\right]+\frac{1}{N}\int_0^D\frac{W(y)}{[1+W(y)]^3}\ln\frac{x}{D}dx + O(1/D)+O(1/N^2),$$

$$y=\frac{D}{\rho V^2}\exp\left(\frac{x+\epsilon_f}{\rho V^2}\right). \tag{B12}$$

4. An analytical expression for the static magnetic susceptibility of the NCA

a. Universality

With the help of the Kondo temperature (14), Eq. (B10) reads, in the magnetic limit $T_K/\rho V^2\to 0$ after the substitution $\omega/T_K=x$,

$$E_0=\epsilon_f-jg\mu_B h-T_K\int_{jg\mu_B h/T_K}^{(D+\epsilon_f)/T_K}dx\frac{1}{1+W\left\{N\exp\left[\sum_m \ln\left(x+\frac{mg\mu_B h}{T_K}\right)\right]\right\}}. \tag{B13}$$

After differentiating with respect to the magnetic field h, the integrand decays rapidly enough so that one can replace the upper limit of integration by ∞. Hence the magnetization scales as a function of h as

$$M(h,D,\epsilon_f,V,N)=M\left(\frac{g\mu_B h}{T_K}\right). \tag{B14}$$

This shows explicitly that already the skeleton diagrams of second order give the exact energy scale for the spin degrees of freedom.

b. Small magnetic fields

Using the parametrization (B10), the magnetization $M(h)=-\partial_h E_0$ vanishes for $h=0$ because of $\Sigma_m m=0$. The second derivative gives the static magnetic susceptibility for $h=0$. With the abbreviation[14]

$$\tfrac{1}{3}\mu_j^2 N=(g\mu_B)^2\sum_m m^2,$$

from Eq. (B10) one has, after substituting $NY_0/\rho V^2=W$, using the NCA differential equations, and finally partially integrating,

$$\chi(0)=\frac{1}{3}\,\mu_j^2\frac{1}{\rho^2V^4}\int_0^D\frac{2W(y)+1}{W(y)[1+W(y)]^3}dx,$$

$$y=\left(\frac{x}{\rho V^2}\right)^{1/N}\frac{T_K}{\rho V^2}\exp\left(\frac{x}{\rho V^2}\right). \tag{B15}$$

In the magnetic limit, y is very small for $x<|\epsilon_f^*|$ because of $-\epsilon_f^*\gg\rho V^2$, and above that $W>1$ and the integrand is small. Therefore one can replace the W function by its argument, and extend the integration to ∞:

$$\chi^{\mathrm{NCA}}(0)=\frac{1}{3}\mu_j^2\frac{1}{T_K}\int_0^\infty e^{-t}t^{-1/N}dt=\frac{1}{3}\mu_j^2\frac{1}{T_K}\Gamma(1-1/N). \tag{B16}$$

The exact result

$$\chi(0)=\frac{1}{3}\mu_j^2\frac{1}{T_K}\frac{1}{\Gamma(1+1/N)} \tag{B17}$$

was obtained by fitting the results of the Bethe ansatz to perturbation theory in the nonmagnetic limit.[5] Both results coincide up to order $1/N$, because the NCA contains all diagrams up to that order. This contradicts the claim of Kuramoto and Kojima[32] that the NCA would yield the exact result for $\chi(0)$ in the magnetic limit.

APPENDIX C: COQBLIN-SCHRIEFFER MODEL

1. Variational functional

The Schrieffer-Wolff transformation[14] projects—up to a constant—the Anderson model onto the Coqblin-Schrieffer model in the magnetic limit $\epsilon_f\to-\infty$, and constant $J=V^2/|\epsilon_f|$,

$$H\mapsto H_{\mathrm{CS}}-2\frac{\rho JD}{N},$$

$$H_{\mathrm{CS}}=\sum_{|\epsilon_p|<D,m}\epsilon_p c_{pm}^+c_{pm}+\frac{J}{N}\sum_{pq,mn}c_{pm}^+c_{qn}f_n^+f_m. \tag{C1}$$

For that the spectrum of H is shifted at $(-\epsilon_f)$ by shifting the argument z in Υ at ϵ_f, and the propagators and self-energies are transformed as[14]

$$\frac{1}{\epsilon_f}\Sigma_0(z+\epsilon_f)\to\Pi(z),$$

$$\frac{1}{1+\dfrac{z}{\epsilon_f}-\dfrac{1}{\epsilon_f}\Sigma_0(z+\epsilon_f)}\to R_0(z)=\frac{1}{1-\Pi(z)},$$

$$R_m(z+\epsilon_f)\to R_m(z)=\frac{1}{z-\Sigma_m(z)}.$$

A $2n$th-order diagram carries the prefactor $(-1)^n(\rho J)^n$. Because $|\epsilon_f|\gg D,|z|$, the term z/ϵ_f was neglected in $\epsilon_f R_0(z+\epsilon_f)$, and such the charge degrees of freedom of the impurity are projected out. The variational functional Υ now reads

$$\Upsilon=\beta\oint\frac{dz}{2\pi i}e^{-\beta z}\Bigg\{\sum_{m,n}\left(1-\frac{1}{n}\right)\Sigma_m^{(n)}(z)R_m(z)+\sum_n\left(1-\frac{1}{n}\right)\Pi^{(n)}(z)R_0(z)+\ln\Bigg[z-\sum_n\Sigma_m^{(n)}(z)\Bigg]+\ln\Bigg[1-\sum_n\Pi^{(n)}(z)\Bigg]\Bigg\}. \tag{C2}$$

The saddle-point property of Υ is shown as by Bickers.[14]

2. Skeleton diagrams of second order

The analog to the NCA is called the ''self-consistent ladder approximation.''[14] The NCA equations follow from Eq. (6) after projecting as in the last paragraph:[14]

$$\Sigma_m(z)=-\frac{\rho J}{N}\int_{-D}^D f(\epsilon)\frac{1}{1-\Pi(z+\epsilon)}d\epsilon,$$

$$\Pi(z)=-\frac{\rho J}{N}\sum_m\int_{-D}^D f(\epsilon)R_m(z+\epsilon)d\epsilon. \tag{C3}$$

The first scaling equation follows as in Sec. III A,

$$F_f=T\frac{\partial}{\partial T}F_f+D\frac{\partial}{\partial D}F_f. \tag{C4}$$

The asymptotic behavior of the self-energies is estimated from Eq. (C3) for $|\omega|\ll D$ as

$$\Sigma_m(\omega-D)=-\rho JD/N+O(J^2),\qquad \Pi(\omega-D)=O(J\ \ln D). \tag{C5}$$

Because of Eq. (C1), z has to be shifted in every propagator by $-2\rho JD/N$, to describe the Coqblin-Schrieffer model. Therefore

$$R_m(\omega-D)=\frac{1}{1+\rho J/N}\frac{-1}{D}\quad\text{for }|\omega|\ll D,\qquad R_0(\omega-D)=1\quad\text{for }|\omega|\ll D. \tag{C6}$$

Higher orders in J are irrelevant as will be shown below. It follows within the NCA that

$$D\frac{\partial}{\partial D}Z_f=-\beta J\oint\frac{dz}{2\pi i}e^{-\beta z}\left(\frac{R_0(z)}{1+\rho J/N}-DR_m(z)\right).$$

Hence the scaling equation for the impurity part of the free energy is

$$D\frac{\partial}{\partial D}F_f^{\mathrm{NCA}}=\frac{(\rho J)^2}{1+\rho J/N}\frac{\partial}{\partial\rho J}F_f^{\mathrm{NCA}}-\frac{\rho J}{N}D. \tag{C7}$$

This equation does not change in the universal limit $J\ll D$ if higher orders of J in Eq. (C6) are taken into account. The following scaling law holds therefore for the impurity part of the free energy:

$$(F_f-E_0)^{\mathrm{NCA}}(T,D,J)=(F_f-E_0)^{\mathrm{NCA}}\left(\frac{T}{T_K^{\mathrm{CS}}}\right), \tag{C8}$$

with the Kondo temperature of the Coqblin-Schrieffer model[2]

$$T_K^{\mathrm{CS}} = D\sqrt[N]{\rho J}\exp[-1/\rho J]. \tag{C9}$$

For other observables, one has to couple H to suitable external fields. In particular, the Kondo resonance is reproduced qualitatively correctly.

3. Skeleton diagrams of higher order

The two limits $D\to\infty$ and $\epsilon_f\to-\infty$ are *not* interchangeable, as can be seen by comparing the Kondo temperatures of Eqs. (14) and (C9). Skeleton diagrams of higher order than two *are* relevant in Υ. The reason for that is the asymptotic behavior of R_0 which goes to *one* at the cutoff. If the diagram in Fig. 3 is logarithmically differentiated with respect to D, the contribution of the second conduction-electron line does not vanish for large D. In particular it is not possible to prove now that the energy scale (C9) is the exact one by considering only skeleton diagrams of second order. In fact, the NCA still predicts for $N=1$ a low-energy scale (C9) although there is none.

4. NCA at zero temperature

The derivations are as in Appendix B. The inverse of the pseudopropagator Π is defined to be $Y_0 = 1-\Pi$. The NCA differential equations are, up to terms $\propto 1/D$,

$$\frac{\partial}{\partial\omega}Y_0 = \frac{-\rho J}{N}\sum_m Y_m^{-1}(\omega), \tag{C10}$$

$$\frac{\partial}{\partial\omega}Y_m = -(1-\rho J/N) - \frac{\rho J}{N}Y_0^{-1}(\omega).$$

With $Y_m = \overline{Y_m} + mg\mu_B h$ and $\widetilde{D} = D(1-\rho J D/N)$ the NCA differential equations have, up to terms of order $1/D$, the integral

$$Y_0\left(\frac{1}{\rho J}-\frac{1}{N}\right) + \frac{1}{N}\ln Y_0 = \frac{1}{N}\sum_m \ln\left|\frac{\overline{Y_m}+mg\mu_B h}{\widetilde{D}}\right| + \left(\frac{1}{\rho J}-\frac{1}{N}\right). \tag{C11}$$

The ground-state energy is expressible as

$$E_0 = -A + \int_{-A}^{E_0} d\omega,$$

where A is a still arbitrary constant. If $J \ll A \ll D$ and $\lim_{D\to\infty} A = \infty$, the integral (C11) can be used as in Appendix B to yield, in the universal limit of small ρJ,

$$\chi^{\mathrm{NCA}}(0) = \frac{1}{3}\mu_j^2 \frac{1}{T_K^{\mathrm{CS}}}\frac{\Gamma(1-1/N)}{\sqrt[N]{e}}. \tag{C12}$$

which is up to $O(1/N^2)$ identical[2] to the result of Rasul and Hewson, where $\Gamma(1-1/N)$ is replaced by $1/\Gamma(1+1/N)$.

[1] G. Grüner and A. Zawadowski, Rep. Prog. Phys. **37**, 1497 (1974).
[2] A. C. Hewson, *The Kondo Problem to Heavy Fermions* (Cambridge University Press, Cambridge, 1993).
[3] N. Andrei, K. Furuya, and J. H. Lowenstein, Rev. Mod. Phys. **55**, 331 (1983).
[4] P. B. Wiegmann and A. M. Tsvelick, Adv. Phys. **32**, 453 (1983).
[5] J. W. Rasul and A. C. Hewson, J. Phys. C **17**, 3337 (1984).
[6] K. G. Wilson, Rev. Mod. Phys. **47**, 773 (1975).
[7] H. Keiter and J. C. Kimball, Phys. Rev. Lett. **25**, 672 (1970).
[8] A. A. Abrikosov and A. A. Migdal, J. Low Temp. Phys. **3**, 519 (1970).
[9] J. M. Luttinger and J. C. Ward, Phys. Rev. **118**, 1417 (1960).
[10] Y. Kuramoto, Z. Phys. B **53**, 37 (1983).
[11] G. Baym, Phys. Rev. **127**, 1391 (1962).
[12] P. Coleman, Phys. Rev. B **29**, 3035 (1984).
[13] P. Fulde, *Electron Correlations in Molecules and Solids* (Springer-Verlag, Berlin, 1995).
[14] N. E. Bickers, Rev. Mod. Phys. **59**, 845 (1987).
[15] N. Grewe, Z. Phys. B **53**, 271 (1983).
[16] Y. Kuramoto, Z. Phys. B **57**, 95 (1984).
[17] F. D. M. Haldane, Phys. Rev. Lett. **40**, 416 (1978).
[18] F. B. Anders, J. Phys. Condens. Matter **7**, 2801 (1995).
[19] H. Keiter and G. Morandi, Phys. Rep. **109**, 227 (1984).
[20] N. E. Bickers, D. L. Cox, and J. W. Wilkins, Phys. Rev. B **36**, 2036 (1987).
[21] E. Müller-Hartmann, Z. Phys. B **57**, 281 (1984).
[22] K. Satori, H. Shiba, O. Sakai, and Y. Shimizu, J. Phys. Soc. Jpn. **61**, 3239 (1992).
[23] D. Withoff and E. Fradkin, Phys. Rev. Lett. **64**, 1835 (1990).
[24] N. Read and D. M. Newns, J. Phys. C **17**, 3273 (1983).
[25] Y. Kuroda and B. Jin, J. Phys. Soc. Jpn. **57**, 1687 (1988).
[26] F. C. Zhang and T. K. Lee, Phys. Rev. B **30**, 1556 (1984).
[27] T. Saso, J. Magn. Magn. Mater. **76&77**, 176 (1988).
[28] J. Kroha, P. J. Hirschfeld, K. A. Muttalib, and P. Wölfle, Solid State Commun. **83**, 1003 (1992).
[29] W. Metzner and D. Vollhardt, Phys. Rev. Lett. **62**, 324 (1989).
[30] E. Müller-Hartmann, Z. Phys. B **74**, 507 (1989).
[31] S. Inagaki, Prog. Theor. Phys. **62**, 1441 (1979).
[32] Y. Kuramoto and H. Kojima, J. Magn. Magn. Mater. **47&48**, 329 (1985).